2013 International Conference on Unmanned Aircraft Systems (ICUAS)
May 28-31, 2013, Grand Hyatt Atlanta, Atlanta, GA

Visual Odometry for Autonomous Outdoor Flight of a Quadrotor UAV

H. Romero*, S. Salazar, O. Santos and R. Lozano

Abstract— **In this paper we propose an alternative approach to estimate the UAV translational velocity and position applying an onboard optical flow sensor. This, is a appropriated sensor to be used in a mini UAV due to its lightness and smallness. With this approach we are able to perform real-time autonomous outdoor and indoor flight without using the GPS information, which in some case is blocked, denied or jammed. Additionally, a PD controller is robustly tuned in order to compensate the uncertain velocity measurements provided by the optical flow sensor. The experimental results obtained by using this approach shown the feasibility of the proposed sensor-controller scheme.**

I. Introduction

The arena of Unmanned Aerial Vehicles (UAV's) has been mainly powered by the defence industry, the main reason is attributed to the complexity and cost of designing, constructing and operating of these vehicles. However, recent advances in micro-electronics especially Micro Electronic Mechanical (MEMS) sensors and the continuing increase of computing capacity and speed together with easy access to better quality composite materials have allowed the design and construction of UAV systems in the domain of civilian and academic users. A UAV can be remotely controlled, semi-autonomous, autonomous or a combination of these. The UAV's are capable to perform a great amount of applications both civilian and military, they can be used to perform inspection in dangerous or polluted environments, highway traffic monitoring, recognition of forest resources, rescue in disaster areas and many more.

Nowadays the mini and micro UAV's are dynamical systems widely studied and developed by many research groups and laboratories around the world, because they can be manipulated and transported by a reduced crew (sometimes only one person), their operational cost is reduced and usually they are simpler to be repaired with respect to the bigger size UAV's. Currently researches developed on mini UAV's are mainly focused on construction, control and instrumentation of these dynamic systems. However these mini aerial system have a limited payload, then the onboard devices (microprocessor and sensors) should be chosen appropriated, such that they must be tiny and light, always considering the energy autonomy level of the UAV and the task to be performed.

* Corresponding author
H. Romero, S. Salazar and R. Lozano are with UMI-LAFMIAA CNRS 3175 CINVESTAV-IPN A.P.14-740 Mexico, D.F. Mexico.
{ssalazar, hromero, rlozano}@ctrl.cinvestav.mx
H. Romero and O. Santos is also with Information Technologies and Systems Research Center, UAEH. 42184 Pachuca, Hgo., Mexico. rhugo, omarj@uaeh.edu.mx

This paper is focused on proposing a navigation strategy based on the optical flow sensor ADNS-3080 [3] with a lens adapted [4] to increase the operating range. This optical information is used to estimate the translational velocity of a mini four-rotor helicopter with respect to a ground in order to stabilize it at hover around a desired set-point. The experimental platform based on optical flow sensor is proposed to be an alternative or a complement to GPS in order to perform autonomous outdoor and indoor flights. This is relevant because in some cases the GPS information is blocked, erroneous or it is not available. The experimental results obtained show a good performance and accuracy (see Figures 4-8), they have been compared versus the GPS information in order to establish a quantitative relation. This platform is also composed by a barometric pressure sensor, configured as altimeter. Moreover, a robust PD controller is proposed to perform hover flight. This controller considers uncertain measurements in the translational variables, it means in the translational positions and velocities.

Fig. 1. Four-rotor UAV in autonomous flight using optical flow measurements.

This work is organized as follows: Previous related works are described in Section II, while in Section III the optical flow equations used to compute the UAV translational velocities are deduced. The dynamical model of flying robot used in this contribution is described in Section IV. The control strategy to stabilize at hover the multi-rotor platform is introduced in Section V. Section VI describes the real-time platform architecture used in this experiment. Finally, experimental results and conclusions are presented in Section VII and Section VIII respectively.

978-1-4799-0817-2/13/$31.00 ©2013 IEEE

II. Related works

Previous works have applied the optical flow for aerial robot stabilization, navigation and landing. In [1] authors used the optical flow measurement obtained from two sideways-looking cameras to estimate the relative distance to obstacles on each side of the helicopter. This visual information was used to develop a proportional control strategy for flying the helicopter along the line between buildings. Furthermore, author in [2] present a navigation strategy that exploits the optical flow information from a single camera to avoid collisions with both lateral and frontal obstacles, it has been tested to control a realistic simulated rotary-wing UAV in a 3D urban textured environment. In this case the authors applied a PID controller to drive the helicopter. A later work [5] proposes a technique combining the optical flow measurements with the stereo vision information in order to have a 3D map of obstacles inside the scene. They are shown that the combination of stereo and optic-flow (stereo-flow) is more effective to navigate in urban canyons than any technique using only one vision sensor.

Other work is [7] where the authors propose a control strategy using the optical flow measurements provided by a monocular vision system to achieve a hover flight that is robust with respect to perturbations like wind. This stabilization strategy was applied to an original configuration of a small aerial vehicle having eight rotors. Moreover, [8] presents a nonlinear controller for a vertical take-off and landing (VTOL) unmanned aerial vehicle (UAV) that exploits a measurement optical flow to enable hover and landing control on amoving platform having a textured flat target plane.

It is important to note that all the above mentioned works have used a camera or a pair of them to estimate the optical flow, which implies a medium or high computational cost (increasing the processing time) for the microprocessor due to image processing tasks. This computational cost could produce an update rate not enough to have a desirable UAV flight performance. For this reason an optical flow sensors based on a low resolution cameras has been used to estimate the translational velocity of flying robot. This sensors are well adapted to payload capabilities of mini UAV's because they are light and small. Some works have applied this technology such as the ADNS-3080 sensor. For instance, authors in [6] show a platform combining this sensor with a camera to stabilize a quadrotor around a desired position and to land on a circular pattern previously designed. It means the experimental test bench is performed in a controlled environment. Moreover, real-time quadrotor stabilization results are presented in [9], authors use the same sensor, which was characterized with respect to Vicon motion capture device in indoor flight.

III. Optical Flow

In this section an analysis of optical flow is developed. Specifically we are interested in how to compute the translational velocity of the flying machine from the optical flow measurements. Optical flow experienced by an on-board sensor (or viewer) can be produced by translational and rotational movements of the flying robot, it means the measured image velocity is directly related with the translational velocity $\mathbf{v}$ and the angular rate ω. In order to deduce the relationships that allows us to determine the robot translational velocity from the optical flow measurements 3 different coordinate frames are defined, such that $\mathcal{I}$ defines the inertial frame, $\mathcal{B}$ is the body frame and $\mathcal{S}$ is the sensor frame. See Figure 2 to $\mathcal{I}$ and $\mathcal{B}$, while $\mathcal{S}$ matches with rows and columns of image sensor array. Under pinhole camera model, a real point p referred to $\mathcal{I}$ is given by

$$p^{\mathcal{I}} = {}^{\mathcal{I}}\mathbf{R}_{\mathcal{B}} p^{\mathcal{B}} + {}^{\mathcal{I}}\mathbf{T}_{\mathcal{B}} \tag{1}$$

where ${}^{\mathcal{I}}\mathbf{R}_{\mathcal{B}}$ is the rotation matrix and ${}^{\mathcal{I}}\mathbf{T}_{\mathcal{B}}$ is the translational vector both from $\mathcal{B}$ to $\mathcal{I}$, while $p^{\mathcal{B}}$ is the real point with respect to $\mathcal{B}$. Moreover the composed velocity (translational and rotational) of a real point $p^{\mathcal{B}}$ is defined as follows

$$\dot{p}^{\mathcal{B}} = -\omega \times p^{\mathcal{B}} - \mathbf{v} \tag{2}$$

which is the motion field referred to body frame $\mathcal{B}$. Nevertheless, the motion field provided by the sensor is referred to the sensor frame $\mathcal{S}$, so it is necessary to apply a transformation between $\mathcal{B}$ and $\mathcal{S}$. Assuming that $\mathcal{B}$ and $\mathcal{S}$ are aligned, therefore they are only related by a scale factor λ such that

$$p^{\mathcal{B}} = \lambda \; p^{\mathcal{S}} \tag{3}$$

then the time derivative is given by

$$\dot{p}^{\mathcal{B}} = \dot{\lambda} \; p^{\mathcal{S}} + \lambda \dot{p}^{\mathcal{S}} \tag{4}$$

Substituting (4) into (2) we get

$$\dot{p}^{\mathcal{S}} = -\omega \times p^{\mathcal{S}} - \frac{\mathbf{v}}{\lambda} - \frac{\dot{\lambda}}{\lambda} p^{\mathcal{S}} \tag{5}$$

this equation shows the dependence of the optical flow (image velocity) from the camera motion ($\mathbf{v}$ and ω) and the depth of the observed point (λ). In order to simplify the problem, assume that the helicopter flights at a well known altitude over piecewise planar surfaces. Also, consider that at hover the yaw angle ψ does not vary, so the optical flow measurements due to rotational movement around the z-axis is zero.

The Avago ADNS-3080 optical flow sensor used in this work delivers an average of optical flow measurement experienced by each one of visual features captured by it both column and row directions. Denote Δ_x and Δ_y the estimated average optical flow in row and column directions respectively. This optical flow measurements are expressed in image coordinate units, it means pixels. The optical flow components $\Delta_{x\dot{\theta}}$ and $\Delta_{y\dot{\phi}}$ produced by the angular rates $\dot{\theta}$ and $\dot{\phi}$ respectively must be compensate to obtain an effective optical flow measurements that reflect the real translational velocity experienced by the flying robot. According to [9], this extra components are defined as follows

$$\Delta_{x\dot{\theta}} = \frac{W_x}{\beta}\ \dot{\theta} \qquad \Delta_{y\dot{\phi}} = \frac{W_y}{\beta}\ \dot{\phi} \tag{6}$$

where W_x is the number of image rows sensor, W_y is the number of image columns of sensor and β denotes the sensor field of view. Angular rates $\dot{\theta}$ and $\dot{\phi}$ are provided by the IMU. Consequently the effective optical flow measurements in pixels are given by

$$\Delta_{xe} = \Delta_x - \Delta_{x\dot{\theta}} \qquad \Delta_{ye} = \Delta_y - \Delta_{y\dot{\phi}} \tag{7}$$

Assuming that the depth of image points λ is equal to the altitude of vehicle h. Therefore, we are able to obtain the measurements in metric units, defined as follows

$$\Delta_{xm} = 2h\frac{\Delta_{xe}}{W_x}\tan\frac{\beta}{2} \qquad \Delta_{ym} = 2h\frac{\Delta_{ye}}{W_y}\tan\frac{\beta}{2} \tag{8}$$

the UAV altitude h is estimated by using a barometric pressure sensor.

IV. Dynamical Model

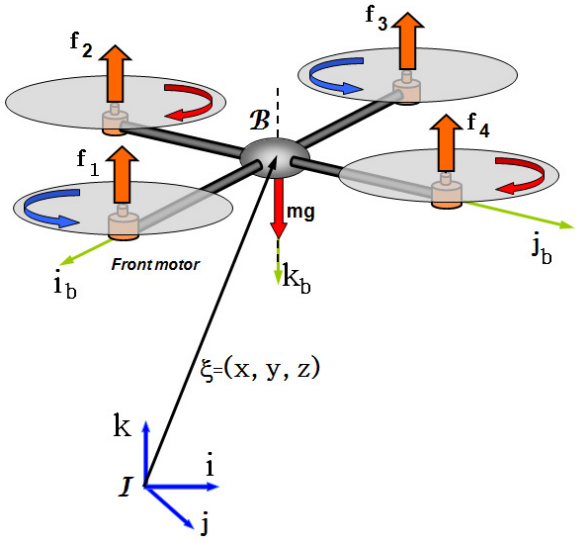

Fig. 2. Four-Rotor Rotorcraft Scheme

The mini flying robot considered in this work is an underactuated dynamical system, provided by four rotors and having 6 degrees of freedom with only 4 control inputs (collective input and roll, pitch and yaw angular moments), a scheme of this flying machine is shown in Figure 2. This system has not nonholonomic constraints, it means, the flying robot has the ability to fly in hover and move omni-directionally in the **3D** space. According to [10], the dynamical model is obtained by Euler-Lagrange formalism and referred to a couple of coordinate frames $\mathcal{I} = \{\hat{i}, \hat{j}, \hat{k}\}$ and $\mathcal{B} = \{\hat{i}_b, \hat{j}_b, \hat{k}_b\}$ defining the inertial and the fixed-body frame respectively. This dynamical model can be separated into translational and rotational parts and it is given as follows

$$\begin{aligned} m\ddot{\xi} &= \mathbf{F}_{\mathcal{I}} + m\mathbf{g} \\ \mathbf{J}\ddot{\eta} &= \tau - \dot{\mathbf{J}}\dot{\eta} + \tfrac{1}{2}\tfrac{\partial}{\partial\eta}\left(\dot{\eta}^T\mathbf{J}\ \dot{\eta}\right) \end{aligned} \tag{9}$$

where vectors $\xi = (x,\ y,\ z)^T$ and $\eta = (\phi,\ \theta,\ \psi)^T$ define the translational and rotational coordinates respectively, m is the mass of the vehicle, $\tau \in \mathbb{R}^3$ denotes the generalized momentum, $\mathbf{J} \in \mathbb{R}^{3\times3}$ represents the positive definite inertia matrix and $\mathbf{g} = (0\hat{i},\ 0\hat{j},\ -g\hat{k})^T$ defines the gravitational acceleration vector. Moreover $\mathbf{F}_{\mathcal{I}} \in \mathbb{R}^3$ is the translational force applied to rotorcraft referred to frame $\mathcal{I}$, specifically $\mathbf{F}_{\mathcal{I}} = {}^{\mathcal{I}}\mathbf{R}_{\mathcal{B}}\mathbf{F}_{\mathcal{B}}$ with the rotation matrix ${}^{\mathcal{I}}\mathbf{R}_{\mathcal{B}}$ relating $\mathcal{B}$ to $\mathcal{I}$ and the total thrust $\mathbf{F}_{\mathcal{B}} = (0\hat{i},\ 0\hat{j},\ \mathbf{u}\hat{k})^T$ referred to body frame $\mathcal{B}$, further details are given in [10].

Assuming that the Coriolis, gyroscopic and centrifugal forces are defined by

$$\mathbf{C}\left(\eta,\dot{\eta}\right)\dot{\eta} = \dot{\mathbf{J}}\dot{\eta} - \tfrac{1}{2}\tfrac{\partial}{\partial\eta}\left(\dot{\eta}^T\mathbf{J}\dot{\eta}\right) \tag{10}$$

then the equation (9) can be rewritten as follows

$$\begin{aligned} m\ddot{\xi} &= \mathbf{F}_{\mathcal{I}} + m\mathbf{g} \\ \mathbf{J}\ddot{\eta} &= \tau - \mathbf{C}\left(\eta,\dot{\eta}\right)\dot{\eta} \end{aligned} \tag{11}$$

Proposing now the following linear feedback for the rotational subsystem

$$\tau = \mathbf{J}\widetilde{\tau} + \mathbf{C}\left(\eta,\dot{\eta}\right)\dot{\eta} \tag{12}$$

with $\widetilde{\tau} = (\tau_\phi,\ \tau_\theta,\ \tau_\psi)^T$, then system (11) becomes to

$$\begin{aligned} m\ddot{\xi} &= \mathbf{F}_{\mathcal{I}} + m\mathbf{g} \\ \ddot{\eta} &= \widetilde{\tau} \end{aligned} \tag{13}$$

Expanding the dynamical model (13) we get

$$m\ddot{x} = -\mathbf{u}\sin\theta \tag{14}$$
$$m\ddot{y} = \mathbf{u}\cos\theta\sin\phi \tag{15}$$
$$m\ddot{z} = \mathbf{u}\cos\theta\cos\phi - mg \tag{16}$$
$$\ddot{\phi} = \widetilde{\tau}_\phi \tag{17}$$
$$\ddot{\theta} = \widetilde{\tau}_\theta \tag{18}$$
$$\ddot{\psi} = \widetilde{\tau}_\psi \tag{19}$$

which is the reduced dynamical model deduced for this flying machine.

V. Robust Stabilizing Control Approach

This section presents the control strategy for stabilizing the four-rotor UAV using the information provided by inertial, optical flow and GPS sensors. In his paper a robust PD controller is synthesized to compensate the uncertainties in the position and velocity variables $(x,\ y,\ z,\ \dot{x},\ \dot{y},\ \dot{z})$ estimated from the optical flow and GPS sensors. The noise presents in the measurements is neglected because a low pass filter is included in the control loop, however the uncertainties in the measurements are always presents. Assuming that the uncertain measurements could be modeled as

$$x_u = x + \delta_x, \qquad y_u = y + \delta_y, \qquad z_u = z + \delta_z$$

$$\dot{x}_u = \dot{x} + \delta_{\dot{x}}, \qquad \dot{y}_u = \dot{y} + \delta_{\dot{y}}, \qquad \dot{z}_u = \dot{z} + \delta_{\dot{z}}$$

where δ_x, δ_y, δ_z, $\delta_{\dot{x}}$, $\delta_{\dot{y}}$ and $\delta_{\dot{z}}$ satisfies the Lipschitz like condition and we assume that these disturbance functions do not grow more quickly that their arguments ($x, \dot{x}, y, \dot{y}, z$ and $\dot{z}$). This assumption could be represented as

$$\begin{array}{lll} |\delta_x| \leq \alpha_x |x| & |\delta_y| \leq \alpha_y |y| & |\delta_z| \leq \alpha_z |z| \\ |\delta_{\dot{x}}| \leq \alpha_{\dot{x}} |\dot{x}| & |\delta_{\dot{y}}| \leq \alpha_{\dot{y}} |\dot{y}| & |\delta_{\dot{z}}| \leq \alpha_{\dot{z}} |\dot{z}| \end{array} \tag{20}$$

where $\alpha_x, \alpha_y, \alpha_z, \alpha_{\dot{x}}, \alpha_{\dot{y}}, \alpha_{\dot{z}} < 1$, which is according to Lipschitz like condition. The robust stability sufficient conditions are established for a PD controller with uncertainties in translational variables (ξ, $\dot{\xi}$) measurements and assuming that inertial variables (η, $\dot{\eta}$) are free of them.

A. Robust stabilization of subsystem z

Consider the non linear controller

$$\mathbf{u} = (\bar{u} + mg) \frac{1}{\cos\theta \cos\phi} \tag{21}$$

proposed in [11] and well defined for $\theta, \phi \in \left(-\frac{\pi}{2}, \frac{\pi}{2}\right)$ and $\bar{u}$ is a PD controller synthesized later. Then, equations (14)-(16) with controller (21) are transformed into

$$m\ddot{x} = -(\bar{u} + mg) \frac{\tan\theta}{\cos\phi} \tag{22}$$

$$m\ddot{y} = (\bar{u} + mg) \tan\phi \tag{23}$$

$$m\ddot{z} = \bar{u} \tag{24}$$

Dealing the $z(t)$ dynamic defined by (24) and defining without loss of generality the reference in the equilibrium point $z, \dot{z} = 0$, then the state space representation for this dynamic is given as follows

$$\begin{aligned} \dot{x}_z &= A_0 x_z + B_0 \bar{u} \\ y_z &= C_0 x_z + F_0(x_z) \end{aligned}$$

where

$$x_z = \begin{bmatrix} z \\ \dot{z} \end{bmatrix} \quad A_0 = \begin{bmatrix} 0 & 1 \\ 0 & 0 \end{bmatrix} \quad B_0 = \begin{bmatrix} 0 \\ 1/m \end{bmatrix}$$

$$y_z = \begin{bmatrix} y_{1z} \\ y_{2z} \end{bmatrix} \quad C_0 = \begin{bmatrix} 1 & 0 \\ 0 & 1 \end{bmatrix} \quad F_0(x_z) = \begin{bmatrix} \delta_z \\ \delta_{\dot{z}} \end{bmatrix} \tag{25}$$

So the control input $\bar{u}$ is proposed as follows

$$\begin{aligned} \bar{u} &= -K_{pz} y_{1z} - K_{dz} y_{2z} \\ &= -K_{pz} z - K_{dz} \dot{z} - K_{pz} \delta_z - K_{dz} \delta_{\dot{z}} \\ &= -K_z x_z - K_z F_0(x_z) \end{aligned} \tag{26}$$

with $K_z = [K_{pz}\ K_{dz}]$. Therefore, the closed loop subsystem is defined by

$$\dot{x}_z = \bar{A}_{0z} x_z - B_{0z} K_z F_0(x_z), \tag{27}$$

where $\bar{A}_0 = A_0 - B_0 K_z$. In order to have a suitable behavior in this subsystem, the vector gains K_z must be chosen such that matrix $\bar{A}_0$ is Hurwitz stable. Using the Lyapunov theory the subsystem stability is determined. So, for the nominal system $\dot{x}_z = \bar{A}_0 x_z$ there exist a matrix $P_z > 0 \in \mathbb{R}^{2\times 2}$ such that the Lyapunov equation

$$P_z \bar{A}_0 + \bar{A}_0^T P_z = -Q_z, \text{ for some } Q_z > 0,$$

is satisfied. It follows that there exist a Lyapunov function $V_0(x_z) = x_z^T P_z x_z$ such that

$$\begin{aligned} \left.\frac{dV_0(x_z)}{dt}\right|_{(27)} &= -x_z^T Q_z x - 2x_z^T P_z B_{0z} K_z F_0(x_z) \\ &\leq -\lambda_{\min}(Q_z) \|x_z\|^2 + 2P_z \|x_z\| \|B_{0z}\| \|K_z\| \|F_0(x_z)\| \\ &\leq -\lambda_{\min}(Q_z) \|x_z\|^2 + 2\bar{\alpha}_{z,\dot{z}} P_z \|x_z\|^2 \|B_{0z}\| \|K_z\| \\ &\leq -\|x_z\|^2 (I_2 \lambda_{\min}(Q_z) - 2\bar{\alpha}_{z,\dot{z}} P_z \|B_{0z}\| \|K_z\|) \end{aligned} \tag{28}$$

where $\bar{\alpha}_{z,\dot{z}} = \min\{\alpha_z, \alpha_{\dot{z}}\}$. Therefore, if the matrix $\lambda_{\min}(Q_z) I_2 - 2\bar{\alpha}_z P_z \|B_{0z}\| \left\|\bar{K}_z\right\|$ is definite positive, then the subsystem (27) is asymptotically robustly stable under uncertainties unstructured measurements z and $\dot{z}$.

B. Robust stabilization of subsystem $y - \phi$

Consider now the subsystem $y - \phi$:

$$\begin{aligned} m\ddot{y}(t) &= (\bar{u} + mg) \tan\phi, \\ \ddot{\phi} &= \widetilde{\tau}_\phi. \end{aligned}$$

The goal for the control $\widetilde{\tau}_\phi$ is to drive the variable ϕ such that it must be suitably small (this will be proved later) in order to assume that $\tan\phi \approx \phi$. Since the closed loop subsystem $z(t)$-$\bar{u}$ is asymptotically robustly stable under uncertain measurements, then for a large enough time $\bar{u} \to 0$. So it leads to

$$\begin{aligned} \ddot{y}(t) &= g\phi, \\ \ddot{\phi} &= \tau_\phi. \end{aligned}$$

where the respective state space representation is defined by

$$\begin{aligned} \dot{x}_{y,\phi} &= A_1 x_{y,\phi} + B_1 \tau_\phi \\ y_{y,\phi} &= C_1 x_{y,\phi} + F_1(y, \dot{y}) \end{aligned} \tag{29}$$

where

$$x_{y,\phi} = \begin{bmatrix} y & \dot{y} & \phi & \dot{\phi} \end{bmatrix}^T \quad A_1 = \begin{bmatrix} 0 & 1 & 0 & 0 \\ 0 & 0 & g & 0 \\ 0 & 0 & 0 & 1 \\ 0 & 0 & 0 & 0 \end{bmatrix}$$

$$B_1 = [0\ \ 0\ \ 0\ \ 1]^T \quad C_1 = \begin{bmatrix} 1 & 0 & 0 & 0 \\ 0 & 1 & 0 & 0 \\ 0 & 0 & 1 & 0 \\ 0 & 0 & 0 & 1 \end{bmatrix}$$

$$F_1(y, \dot{y}) = [\delta_y \quad \delta_{\dot{y}} \quad 0 \quad 0]^T \quad y_{y,\phi} = \begin{bmatrix} y_{1y,\phi} \\ y_{2y,\phi} \end{bmatrix}$$

Let τ_ϕ be a PD controller (with the reference in zero) considering uncertainties in the measurements of y and $\dot{y}$ defined by

$$\tau_\phi = -K_{y,\phi} x_{y,\phi} - K_{y,\phi} F_1(y, \dot{y}) \tag{30}$$

where $K_{y,\phi} = [K_{py} \quad K_{d,\dot{y}} \quad K_{p\phi} \quad K_{d,\dot{\phi}}]$ and $F_1(y,\dot{y}) = [\delta_y \quad \delta_{\dot{y}} \quad 0 \quad 0]^T$. The closed loop system (29)-(30) is given by

$$\dot{x}_{y,\phi} = \bar{A}_1 x_{y,\phi} - B_1 K_{y,\phi} F_1(y,\dot{y}),$$

where $\bar{A}_1 = A_1 - B_1 K_{y,\phi}$ and vector $K_{y,\phi}$ must be chosen such that matrix $\bar{A}_1$ is Hurwitz stable. Consequently for the system $\dot{x}_{y,\phi} = \bar{A}_1 x_{y,\phi}$ there exist a matrix $P_{y,\phi} > 0$ such that satisfies the Lyapunov equation $P_{y,\phi}\bar{A}_1 + \bar{A}_1^T P_{y,\phi} = -Q_{y,\phi}$, for some $Q_{y,\phi} > 0$. Then, we can construct a Lyapunov function $V_1(x_{y,\phi}) = x_{y,\phi}^T P_{y,\phi} x_{y,\phi}$ such that

$$\begin{aligned} &\left.\frac{dV_1(x_{y,\phi})}{dt}\right|_{(29)} \\ &= -x_{y,\phi}^T Q_{y,\phi} x_{y,\phi} - 2x_{y,\phi}^T P_{y,\phi} B_1 K_{y,\phi} F_1(y,\dot{y}) \\ &\leq -\|x_{y,\phi}\|^2 \left(I_4 \lambda_{\min}(Q_{y,\phi}) - 2\bar{\alpha}_{y,\dot{y}} P_{y,\phi} \|B_1\| \|K_{y,\phi}\|\right) \end{aligned} \tag{31}$$

where $\bar{\alpha}_{y,\dot{y}} = \min\{\alpha_y, \alpha_{\dot{y}}\}$, so if the matrix $\left(\lambda_{\min}(Q_{y,\phi})I_4 - 2\bar{\alpha}_{y,\dot{y}} P_{y,\phi} \|B_1\| \left\|\bar{K}_{y,\phi}\right\|\right)$ is definite positive, then the subsystem (29) is asymptotically robustly stable under uncertainties unstructured measurements y and $\dot{y}$. Consequently, our supposition about $\tan\phi \approx \phi$ it is true if $\left(\lambda_{\min}(Q_{y,\phi})I_2 - 2\bar{\alpha}_{y,\dot{y}} P_{y,\phi} \|B_1\| \left\|\bar{K}_{y,\phi}\right\|\right) > 0$.

C. Robust stabilization of subsystem $x - \theta$

Now, consider the system

$$\begin{aligned} m\ddot{x} &= -(\bar{u} + mg)\frac{\tan\theta}{\cos\phi} \\ \ddot{\theta} &= \tilde{\tau}_\theta. \end{aligned}$$

As proved above, the trajectory ϕ is asymptotically stable, then we consider that $\cos\phi \approx 1$ and we want to obtain a PD controller $\tilde{\tau}_\theta$ which assures that $\tan\theta \approx \theta$ it means $\theta \to 0$. With these assumptions together with $\bar{u} \to 0$ we obtain the following simplified subsystem

$$\begin{aligned} \ddot{x} &= -g\theta \\ \ddot{\theta} &= \tilde{\tau}_\theta, \end{aligned} \tag{32}$$

which has the following state space representation

$$\begin{aligned} \dot{x}_{x,\theta} &= A_2 x_{x,\theta} + B_2 \tau_\theta \\ y_{x,\theta} &= C_2 x_{x,\theta} + F_2(x,\dot{x}) \end{aligned} \tag{33}$$

where

$$x_{x,\theta} = \begin{bmatrix} x & \dot{x} & \theta & \dot{\theta} \end{bmatrix}^T \quad A_2 = \begin{bmatrix} 0 & 1 & 0 & 0 \\ 0 & 0 & -g & 0 \\ 0 & 0 & 0 & 1 \\ 0 & 0 & 0 & 0 \end{bmatrix}$$

$$B_2 = [0 \quad 0 \quad 0 \quad 1]^T \quad C_2 = \begin{bmatrix} 1 & 0 & 0 & 0 \\ 0 & 1 & 0 & 0 \\ 0 & 0 & 1 & 0 \\ 0 & 0 & 0 & 1 \end{bmatrix}$$

$$F_2(y,\dot{y}) = [\delta_x \quad \delta_{\dot{x}} \quad 0 \quad 0]^T \quad y_{x,\theta} = \begin{bmatrix} y_{1x,\theta} \\ y_{2x,\theta} \end{bmatrix}$$

Similarly, the PD controller for this subsystem is given as follows

$$\tau_\theta = -K_{x,\theta} x_{x,\theta} - K_{x,\theta} F_3(x,\dot{x}) \tag{34}$$

where $K_{x,\theta} = \begin{bmatrix} K_{px} & K_{d,\dot{x}} & K_{p\theta} & K_{d,\dot{\theta}} \end{bmatrix}$ and $F_3(x,\dot{x}) = [\delta_x \quad \delta_{\dot{x}} \quad 0 \quad 0]^T$. Now one can choose the vector $\bar{K}_{x,\theta}$ such that the matrix $\bar{A}_2 = A_2 - B_2\bar{K}_{x,\theta}$ is Hurwitz stable. So, there exist a matrix $P_{x,\theta} > 0$ such that satisfies the Lyapunov equation $P_{x,\theta}\bar{A}_2 + \bar{A}_2^T P_{x,\theta} = -Q_{x,\theta}$, for some $Q_{x,\theta} > 0$. Then, building the Lyapunov function $V_2(x_{x,\theta}) = x_{x,\theta}^T P_{x,\theta} x_{x,\theta}$ such that

$$\begin{aligned} &\left.\frac{dV_2(x_{x,\theta})}{dt}\right|_{(33)} \\ &= -x_{x,\theta}^T Q_{x,\theta} x_{x,\theta} - 2x_{x,\theta}^T P_{x,\theta} B_2 K_{x,\theta} F_2(x,\dot{x}) \\ &\leq -\|\bar{x}_{x,\theta}\|^2 \left(I_4 \lambda_{\min}(Q_{x,\theta}) - 2\bar{\alpha}_{x,\dot{x}} P_{x,\theta} \|B_2\| \left\|\bar{K}_{x,\theta}\right\|\right) \end{aligned} \tag{35}$$

where the matrix $\left(\lambda_{\min}(Q_{x,\theta})I_4 - 2\bar{\alpha}_{x,\dot{x}} P_{x,\theta} \|B_2\| \left\|\bar{K}_{x,\theta}\right\|\right)$ is definite positive and $\bar{\alpha}_{x,\dot{x}} = \min\{\alpha_x, \alpha_{\dot{x}}\}$. Therefore the subsystem (33) is asymptotically robustly stable under uncertainties unstructured measurements x and $\dot{x}$ and $\tan\theta \approx \theta$.

D. Stabilization of subsystem ψ

Finally, consider the subsystem

$$\ddot{\psi} = \tau_\psi,$$

the state space representation for this subsystem is

$$x_\psi = A_3 x_\psi + B_3 \tau_\psi, \tag{36}$$

where

$$\bar{x}_\psi = \begin{bmatrix} \psi & \dot{\psi} \end{bmatrix}^T, \; A_3 = \begin{bmatrix} 0 & 1 \\ 0 & 0 \end{bmatrix}, \; B_3 = \begin{bmatrix} 0 \\ 1 \end{bmatrix}, \tag{37}$$

Similar arguments are considered in order to obtain a PD controller in the form

$$\tau_\psi = -K_{p,\psi}\psi - K_{d,\dot{\psi}}\dot{\psi}, \tag{38}$$

such that the closed loop system (36) is stable.

We can summarize these sufficient conditions for the robust stability in the following proposition:

Proposition 1

The system represented in the equations (14)-(19) is robustly asymptotically stable with control laws defined by (21), (26), (30), (34) and (38) under uncertainties measurements in ξ and $\dot{\xi}$ given by (20), if the inequalities (28), (31) and (35) are satisfied.

In order to verify the conditions (28), (31) and (35), the controllers gains have been chosen with the values shown in Table 39

K_{px}	$K_{d\dot{x}}$	K_{py}	$K_{d\dot{y}}$	K_{pz}	$K_{d\dot{z}}$
1.5	4.0	1.0	2.0	1.2	2.0
$K_{p\theta}$	$K_{d\dot{\theta}}$	$K_{p\phi}$	$K_{d\dot{\phi}}$	$K_{p\psi}$	$K_{d\dot{\psi}}$
1.5	4.0	1.0	3.0	1.7	2.3

(39)

These values are used in the experiments later. The conditions (28), (31) and (35) are satisfied with the following values for $\alpha_z, \alpha_y, \alpha_x, \alpha_{\dot{z}}, \alpha_{\dot{y}}$ and $\alpha_{\dot{x}}$:

$\bar{\alpha}_{z,\dot{z}}$	$\bar{\alpha}_{y,\dot{y}}$	$\bar{\alpha}_{x,\dot{x}}$
0.13	0.03	0.02

System (37) is stable when values $K_{p\psi} = 1.7$ and $K_{d\dot{\psi}} = 2.3$ are employed in the corresponding PD controller.

VI. Experimental Testbed

The miniature quad-rotor is powered by four brushless motors with fixed pitch propellers. Altitude is controlled by the collective thrust of the motors. The pitch motion is achieved through the difference between forces f_1 and f_3, while the vehicle roll position is controlled by the difference between forces f_2 and f_4 as is shown in Figure 2. The total weight of the vehicle is about 500 gr, with a flight endurance of 25 minutes approximately.

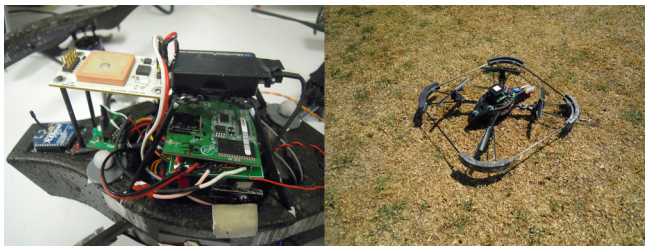

Fig. 3. Testbed experimental plateforme.

Theoretical results obtained were incorporated into an autopilot control system using an architecture based on a 59 MHz Rabbit microcontroller with 1024 Kb Flash and up 2 GB RAM. These microcontrollers are capable of handling floating point operations and multitasking processing virtually due to the enhancement compiler Dynamic C. We have use a commercial inertial measurement unit (IMU) composed by 1 compass, 3 accelerometers and 3 gyros to obtain the roll, pitch and yaw angles and angular rates. Also the embedded autopilot uses a GPS antenna Ublox LEA-6S, modem Xbee, optical flow sensors and radio receiver (See Figure 3).

The optical flow sensor is the ADNS-3080 with 8 mm adapted lens, this sensor includes an internal low-resolution camera and a digital signal processor (DSP) programmed to estimate the relative displacement of the micro shadows of the images acquired. The sensor computes the optical flow by performing a comparative analysis of the sequence of images acquired of a flat surface in front of the sensor in order to estimate the relative motion between the sensor and surface. The optical flow estimation is performed by one-directional correlation algorithm. This sensor is controlled via 4 wires SPI port.

The IMU and visual information are sent to the microcontroller which also reads the input reference through a serial connections. The microcontroller subsequently combines this information to compute the control signals and sends the control corrections to the motors through an I2C serial port. Hence, the brushless motor speed controllers or boosters are handled by the I2C port of the microcontroller.

VII. Experimental Results

The control strategy for this vehicle is a robust control law where the position and velocity of the vehicle are estimated using a optical flow information as was explained in the previous sections. The closed loop system includes a low pass filter of the X and Y optical flow estimated velocities. First a GPS reference calibration was performed in order to assure the correct velocities estimation. We fixed the altitude al $Z_d = 1.5m$ and the angle $\alpha = 90$. The experimental results are shown in figures 4-5.

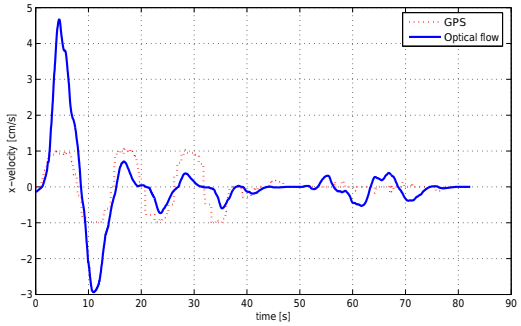

Fig. 4. X velocity estimation.

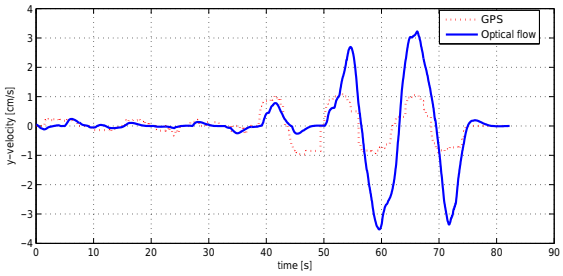

Fig. 5. Y velocity estimation.

The experiment was developed using the four rotor rotorcraft, we started in $x, y, z = 0, 0, 1.5m$ and a square trajectory was proposed. In our algorithm we are using a complementary filter using only the estimated velocities in x and y axes to estimate the x and y position. We performed a discrete integral to obtained the position and we used the estimated velocity in the complementary filter. The experimental results are shown in the Figure 6, we observed that the optical flow approach is closed at approach using GPS antenna.

In Figure 7 the UAV position at hover is shown, while the velocities are plotted in Figure 8.

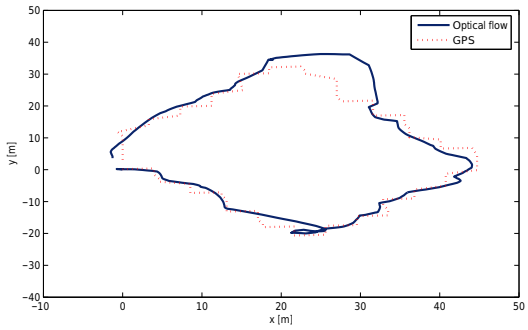

Fig. 6. X-Y position estimation in tracking trajectory evolution.

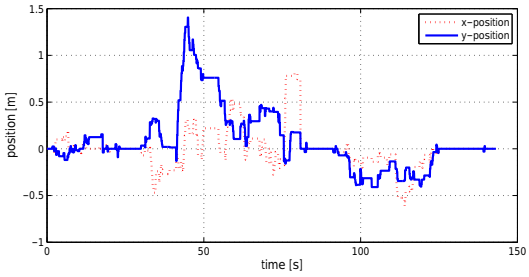

Fig. 7. X and Y position of UAV at hover flight.

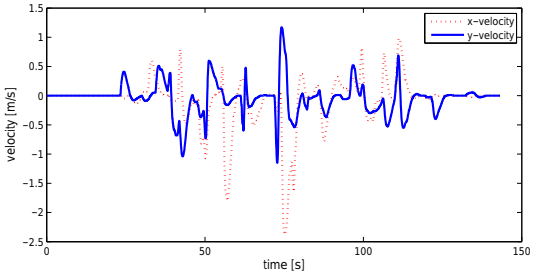

Fig. 8. X and Y velocities of UAV at hover flight.

To adjust the control parameters several flight tests were carried out until obtaining a good performance of the vehicle.

VIII. Conclusions

A visual odometry approach was proposed using optical flow measurements. This approach is an alternative to perform autonomous outdoor navigation, when the GPS signals are not available. Also a robust control was proposed, this control law considers uncertain measurement in the translational states provided by the visual and pressure sensors. The experimental result show a valid strategy to perform outdoor navigation without GPS information. This kind of sensor is well adapted to be used in aerial robots with limited payload because it is tiny and light.

References

[1] Hrabar, S. E. and G. S. Sukhatme, *A comparison of two camera configurations for optic-flow based navigation of a uav through urban canyons*. In Proc. of International Conference on Intelligent Robots and Systems IROS 04, pp. 2673-2680, Sendai Japan 2004.

[2] L. Muratet, S. Doncieux and J. A. Meyer, *A biometric navigation system using optical flow for a rotary-wing uav in urban environment*. In Proc. of International Conference on Intelligent Robots and Systems IROS 04, Sendai Japan 2004.

[3] http://www.avagotech.com/pages/home/. Visited in January 2013.

[4] https://store.diydrones.com/, optical flow sensor based on ADNS-3080 sensor. Visited in January 2013.

[5] S. Hrabar, G. S. Sukhatme, P. Corke K. Usher and J. Roberts, *Combined optic-flow and stereobased navigation of urban canyons for a UAV*. In Proc. of International Conference on Intelligent Robots and Systems IROS 05, pp. 33093316, Edmonton Canada 2005.

[6] S. Lange, N. Sunderhauf, and P. Protzel, *A vision based onboard approach for landing and position control of an autonomous multirotor uav in gps-denied environments*. In Proceedings of the Int. Conf. on Advanced Robotics ICAR 09. pp. 1-6, Munich, Germany 2009.

[7] Hugo Romero, Sergio Salazar and Rogelio Lozano, *Real-Time Stabilization of an Eight-Rotor UAV Using Optical Flow*. IEEE Transaction on Robotics, vol. 25 no. 4, pp. 809-817, 2009.

[8] B. Herissé, T. Hamel, R. Mahony, and F.X. Russotto, *Landing a VTOL Unmanned Aerial Vehicle on a Moving Platform Using Optical Flow*. IEEE Transactions on Robotics, vol. 28, no. 1, pp. 77-89, 2012.

[9] Hyon Lim, Hyeonbeom Lee and H. Jin Kim, *Onboard Flight Control of a Micro Quadrotor Using Single Strapdown Optical Flow Sensor*. In Proc. of International Conference on Intelligent Robots and Systems IROS 12, pp. 495-500, Vilamoura, Algarve Portugal 2012.

[10] H. Romero, S. Salazar and R. Lozano, *Visual servoing applied to real-time stabilization of a multi-rotor UAV*. Robotica Cambridge Press. vol. 30, no. 7, pp. 1203-1212, 2012.

[11] P. Castillo, A. Dzul and R. Lozano, *Real-Time Stabilization and Tracking of a Four Rotor Mini Rotorcraft*. IEEE Transactions on Control Systems Technology, Vol. 12, No. 4, pp. 510-516, 2004.